DOI: 10.1002/anie.201107817

Lithium–Sulfur Battery

Spherical Ordered Mesoporous Carbon Nanoparticles with High Porosity for Lithium–Sulfur Batteries**

Jörg Schuster, Guang He, Benjamin Mandlmeier, Taeeun Yim, Kyu Tae Lee, Thomas Bein, and Linda F. Nazar**

Rechargeable lithium–sulfur (Li–S) batteries are attracting increasing attention due to their high theoretical specific energy density, which is 3 to 5 times higher than that of Li-ion batteries based on intercalation chemistry.[1] Since the electronic conductivity of sulfur is extremely low,[2] conductive carbon materials with high accessible porosity to "wire" and contain the sulfur are an essential component of the positive electrode. During the past decades, attempts have been made to fabricate C/S composites using carbon black,[3] activated carbons (ACs),[4] and carbon nanotubes (CNTs).[5] Although improvements resulted, the cathodes suffered from inhomogeneous contact between the active material and the electronic conductors. A major step forward in fabricating a uniform C/S composite was reported in 2009. Some of us employed CMK-3, an ordered mesoporous carbon (OMC) featuring high specific surface area and large pore volume as a scaffold.[6] As much as 70 wt % sulfur was incorporated into the uniform 3–4 nm mesopores, and the cells exhibited reversible capacities up to 1350 mA h g^{-1}, albeit at moderate rates. Inspired by this, another OMC, a bulk bimodal mesoporous carbon (BMC-1) was investigated as a Li-S cathode.[7] The favorable pore dimensions and large pore volume greatly improved the rate performance. An electrode with 40 wt % S showed a high initial discharge capacity of 1135 mA h g^{-1} at a current rate of 1 C (defined as discharge/charge in one hour). However, similar to other reports,[2b,8] the capacity is sensitive to the sulfur ratio, dropping to 718 mA h g^{-1} at a sulfur content of 60 wt %. These results suggest that the texture of the mesoporous carbon could be further enhanced. Recently, Archer et al. reported nanoscale hollow porous C/S spheres prepared through vapor infusion.[9] These materials displayed good cyclability and capacity at a C/5 rate, illustrating the advantages of nanosized porous carbon in the sulfur cathodes.

Here we report the synthesis of unique nanoscale spherical OMCs with extremely high bimodal porosities. The particles were investigated as a cathode material and sulfur host in Li–S batteries where they showed high initial discharge capacity and good cyclability without sacrificing rate capability. Unlike bulk porous carbons, these carbon–sulfur sphere electrodes did not display significant capacity fading with the increase of sulfur content in the cathodes. We show that the nanoscale morphology of these materials is of key importance for ensuring very efficient use of the sulfur content even at high cycling rates. Morphology control is a central issue in OMC[10] synthesis. There are numerous examples of mesoporous bulk materials obtained either by hard-templating[11] or soft-templating,[12] including thin films,[13] membranes[14] or free fibers.[14c,15] Most syntheses use evaporation-induced self-assembly (EISA) followed by thermal treatment for template-removal and carbonization. It is a challenge to either create solution-based OMC nanoparticle syntheses or to adapt the established EISA methods to nanoparticles.

Only few examples of OMC nanoparticles have been reported so far which are mostly unsuitable for applications in Li–S cells due to low pore volume and/or surface area. Approaches include templating with PMMA colloidal crystals[16] or mesoporous silica nanoparticles,[17] aerosol-assisted synthesis,[18] ultrasonic emulsification[19] or hydrothermal synthesis.[20] Ordered arrays of fused mesoporous carbon spheres were reported by Liu et al. using a macroporous silica as template.[21] Recently Lei et al.[22] reported the synthesis of 65 nm mesoporous carbon nanospheres, with both 2.7 nm mesopores and high textural porosity (surface area of 2400 $m^2 g^{-1}$). These showed promising supercapacitor properties.

Our spherical OMC nanoparticles of 300 nm in diameter, prepared by a novel method, can be dispersed in water by sonification to form stable colloidal suspensions. The spherical mesoporous carbon nanoparticles were obtained in a two-step casting process. An opal structure of PMMA spheres was cast with a silica precursor solution to form a silica inverse opal. The inverse opal was then used as template for a triconstituent precursor solution containing resol as the carbon precursor, tetraethylorthosilicate (TEOS) as the silica precursor and the block copolymer Pluronic F127 as a structure-directing agent.[12a] Carbonization was followed by etching of the silica template and the silica in the carbon/silica nanocomposite, resulting in the formation of OMC with hierarchical porosity. Through the presence of silica in the

[*] J. Schuster,[+] B. Mandlmeier, Prof. Dr. T. Bein
Department of Chemistry and Center for NanoScience (CeNS), University of Munich (LMU), Butenandtstrasse 5–13 (Gerhard Ertl Building), 81377 Munich (Germany)
E-mail: tbein@cup.uni-muenchen.de
Homepage: http://bein.cup.uni-muenchen.de
G. He,[+] T. Yim, K. T. Lee, Prof. Dr. L. F. Nazar
Department of Chemistry, University of Waterloo
200 University Avenue West, Waterloo, Ontario N2L 3G1 (Canada)
E-mail: lfnazar@uwaterloo.ca
[+] These authors contributed equally to this work.

[**] The authors thank NSERC (Canada), the NIM cluster (DFG), CeNS, and the DFG (SFB 486) for support of this work. We thank Tina Reuther for nitrogen sorption measurements.
Supporting information for this article is available on the WWW under http://dx.doi.org/10.1002/anie.201107817.

walls, shrinkage during carbonization is reduced and additional porosity is produced by its removal; therefore very high mesoporosity is created. To the best of our knowledge the material shows the highest inner pore volume for mesoporous carbon nanoparticles of 2.32 $cm^3 g^{-1}$ and also one of the highest surface areas of 2445 $m^2 g^{-1}$ with a bimodal pore size distribution.

The scanning electron microscopy (SEM) images in Figure 1 depict the morphologies at different steps of the synthesis. The 400 nm PMMA spheres, close packed in an opal structure, (Figure 1a) were used as the template for a silica precursor solution. A highly ordered inverse silica opal structure (Figure 1b) was formed after calcination. The silica was then used in a second casting step as a template for an artificial opal made of OMC spheres (Figure 1c,d). The particle size of the OMC spheres (Figure 1c) is around 300 nm, indicating little shrinkage occurred at 900 °C. The OMC spheres exhibit the close packing of the PMMA spheres and the silica inverse opal. The representative TEM micrographs in Figure 1d,e reveal their 2D-hexagonal mesostructure (*P6mm*). In agreement with the SEM results, the mean particle size was (300 ± 40) nm. Figure 1d depicts the hexagonal structure projected along the columns. The FFTs clearly show the hexagonal symmetry of the projections with *d*-spacings of 12.5 nm. Tilting up to 30° showed no other zone axes; this excludes a 3D structure and verifies the 2D-hexagonal mesostructure. Figure 1e shows the 2D-hexagonal structure tilted out of the columnar projection, where the cylindrical pores can be clearly observed. Thus the spherical

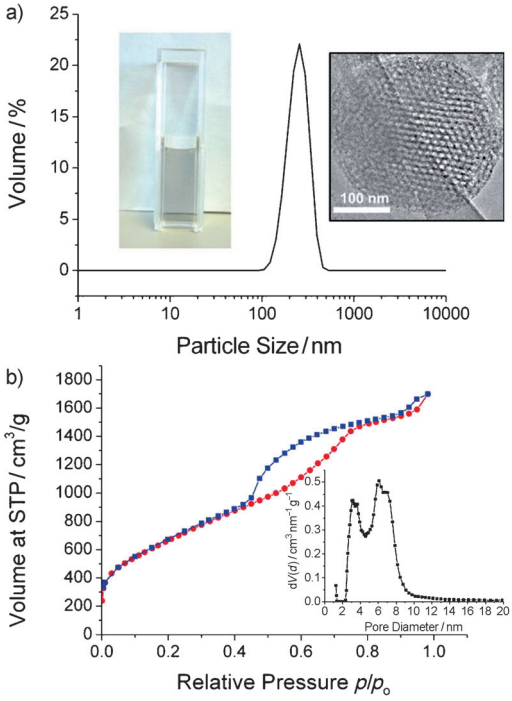

Figure 2. a) DLS measurement of OMC spheres in water after sonification with insets of the stable colloidal suspension and a TEM micrograph showing the intact 2D-hexagonal mesostructure. b) Nitrogen sorption isotherm and pore size distribution (inset, NLDFT adsorption branch) of the spherical OMC nanoparticles.

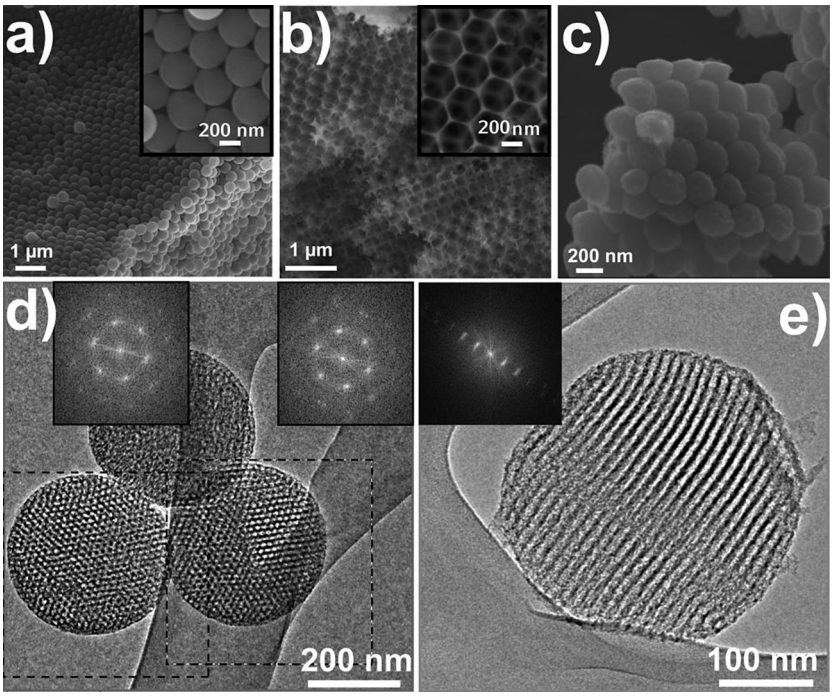

Figure 1. SEM images: a) PMMA spheres ordered in close packing with an inset at higher magnification. b) Silica inverse opal structure with an inset at higher magnification. c) OMC spheres ordered in opal structure. d,e) TEM micrographs of spherical OMC nanoparticles showing the 2D-hexagonal structure: d) projected along the columns, with insets of fast Fourier transforms (FFT) of the squares; e) tilted out of the columnar projection with FFT inset.

nanoparticles exhibit the same structure as the bulk material described by Liu and coworkers[12a] synthesized from a similar precursor solution. On grinding for TEM preparation, the OMC opal aggregates separated into small clusters (e.g. in Figure 1d) or even single particles (e.g. in Figure 1e), indicating that they are only loosely bound. Complete separation could be achieved by sonification.

The dynamic light scattering (DLS) measurement in Figure 2a shows an average particle size of 255 nm and a narrow size distribution. The mean particle size here is even smaller than found in SEM and TEM (300 nm). Thus the spheres could be isolated from the close packing of the opal structure to form stable colloidal suspensions of single nanoparticles. The left inset shows a colloidal suspension of the spheres in water, which was still stable after one week. The TEM micrograph in the right inset shows that even after the relatively harsh ultrasonic treatment the particles still exhibit a 2D-hexagonal mesostructure. The OMC spheres show excellent porosity properties as illustrated in Figure 2b. They exhibit a Type IV isotherm with a Brunauer–Emmett–Teller (BET) surface area of

2445 $m^2 g^{-1}$, an inner pore volume of 2.32 $cm^3 g^{-1}$ (p/p_0=0.82, pores < 13 nm), and a total pore volume of 2.63 $cm^3 g^{-1}$ (p/p_0 = 0.98). The bimodal pore size distribution (NLDFT adsorption branch) shows a maximum for large pores of 6.0 nm and smaller pores (3.1 nm). The latter arise from the porous walls formed by etching the silica from the carbon/silica nanocomposite walls.

Three C/S samples denoted as S-BMC/S-50, S-BMC/S-60, and S-BMC/S-70 were prepared (spherical-bimodal mesoporous carbon). The sulfur content of each sample was confirmed (Figure S1 a, Supporting Information) by thermogravimetric analysis (TGA): 49.7 wt%, 61.4 wt%, and 70.0 wt%, respectively, and BET analysis of the sample exhibited the expected decrease in pore volume with increase in sulfur content (Figure S2). Elemental maps of a single spherical carbon–sulfur particle (Figure S3) show that sulfur was homogeneously distributed into the pores. S-BMC/S-50 shows the highest reversible discharge capacity of 1200 mA h g^{-1} (Figure S4 a). After 100 cycles this cell maintained a capacity of 730 mA h g^{-1} at a high current density of 1 C (1675 mA g^{-1}; see Experimental Section for details). Strikingly, unlike in previous reports,[2b,7a,8,23] the electrochemical performance of the C/S nano composites was not strongly affected by increasing the sulfur content to 60 and 70 wt%. Both S-BMC/S-70 (Figure 3 a) and S-BMC/S-60 (Figure S4 a) display an initial capacity of about 1070 mA h g^{-1} with 700 mA h g^{-1} retained after 100 cycles, comparable to S-BMC/S-50.

All three materials show a drop in capacity during the first two cycles, followed by good stability on subsequent cycling. This is explained by the probable formation of a thin S layer on the external surface of the carbon nanospheres, owing to the strong affinity of sulfur for carbon.[6,24] This is significant since their proportion of external surface area to pore surface area is relatively large. It is also consistent with the initial charge–discharge profile of S-BMC/S-70 (Figure 3 b, black curve). An overcharge capacity of about 150 mA h g^{-1} is observed, which we attribute to the dissolution of the reduced surface polysulfide species which engage in the shuttle mechanism during the electrode redox reactions (the results of the other two samples, which are not shown, are similar). In order to overcome this, two approaches were followed. First, S-BMC/S-70 was treated with CS_2 to remove excess external sulfur. TGA data (Figure S1 b) indicated that about 14% of the sulfur was extracted. Nonetheless, the content is still higher of that of many other composites.[2b,8,23,24b] The blue curve in Figure 3 b shows that all of the overcharge capacity disappeared in the first cycle of the washed ("S-BMC/S-70-W") sample, indicating that the undesired shuttle processes are suppressed. The sharp capacity drop at the 2nd cycle was also diminished (Figure 3 a). This material retained a capacity above 830 mA h g^{-1} after 100 cycles at a current rate of 1 C (i.e., 83% capacity retention). Some overcharge (ca. 95 mA h g^{-1}) appeared on the course of cycling as shown in Figure 3 c, similar to that reported for hollow carbon–sulphur composites.[9] The coulombic efficiency dropped from 100% on the first cycle to 92% after 10 cycles, but remained relatively constant thereafter, indicating reliable stability. Relative to S-BMC/S-50 and S-BMC/S-60 (Figure S4) (with similar sulfur content) it showed the best results. We anticipate even better capacity retention would be achieved with surface protection of the negative electrode.

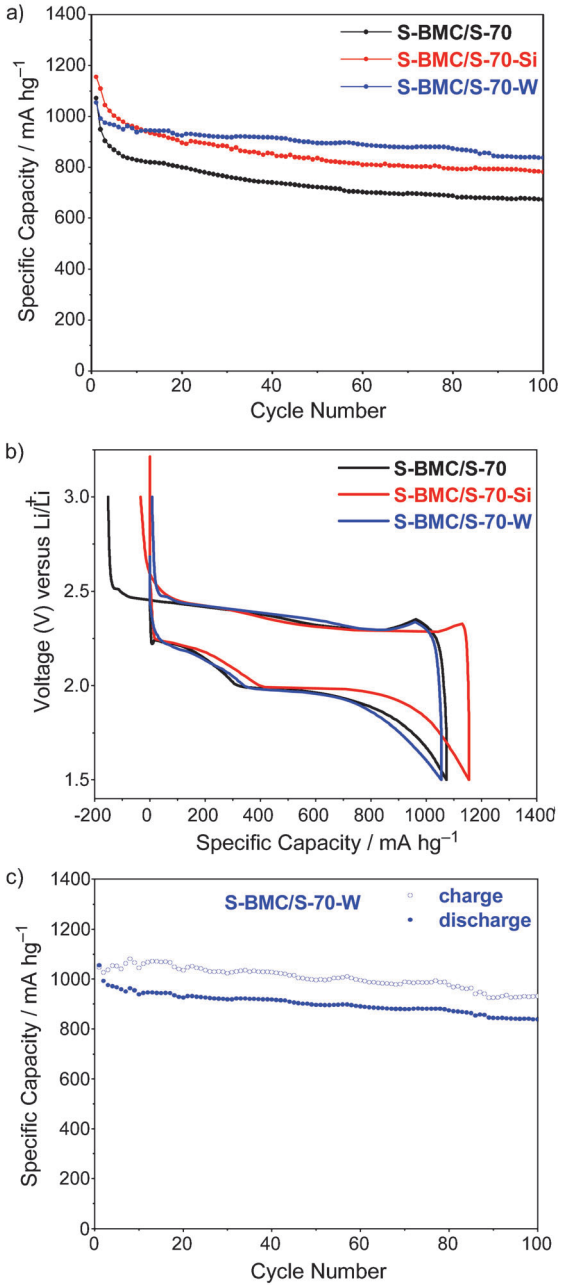

Figure 3. a) Cycling stability of the three 70 wt% C/S electrodes, as prepared (S-BMC/S-70), washed (S-BMC/S-70-W) and SiO_x-coated (S-BMC/S-70-Si). b) Comparison of initial charge–discharge profiles of as-prepared S-BMC/S-70 versus post-treated samples by SiO_x coating or CS_2 washing. c) Discharge and charge capacity of S-BMC/S-70-W as a function of cycle number. All the cells were operated at a current rate of 1 C (1675 mA g^{-1}) at room temperature.

Another approach to avoid overcharge was to modify the sample S-BMC/S-70 with a thin SiO_x coating. It has been established that additives can play important roles in the sulfur electrodes to suppress the polysulfide shuttle,[25] among which mesoporous silica is particularly promising.[26] Very

recently, some of us have also developed another facile method by creating a thin SiO_x layer on the surface of the C/S electrodes.[27] The electrochemical data for the functionalized sample S-BMC/S-70-Si (Figure 3 a,b) shows that the homogeneous SiO_x coating evident in the TEM EDX map (Figure S5, ca. 2 wt% SiO_x by TGA, Figure S6) was effective and that most of the over-discharge capacity was eliminated. The coating does not significantly affect the conductivity of the cathode as determined by impedance measurements (Figure S7). The efficacy of the coating approach was also reflected by the improved long-term cycling performance (Figure S4 b). Comparison of the nanospherical S-BMC bimodal mesoporous carbon with the previously investigated bulk material BMC-1 is illustrated in Figure 4, which clearly

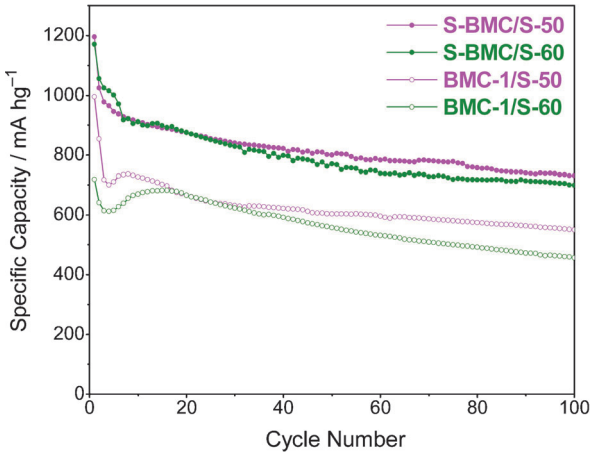

Figure 4. Comparison of electrodes prepared from BMC-1 and S-BMC showing the importance of particle size on the electrochemical performance. All the cells were operated at a current rate of 1 C (1675 mA g^{-1}) at room temperature.

demonstrates the advantages of S-BMC. The more sulfur is incorporated, the more obvious is the advantage. The small particle size of S-BMC allows the sulfur to distribute more homogeneously into the pores, which greatly enhances the electrochemical behavior of the corresponding electrodes, compared with the bulk mesoporous carbon BMC-1. It is also of interest to contrast these nano, bimodal pore (3/6 nm) S-BMC materials with our previously reported CMK-3 sulfur composites that were based on a single pore size of 3.3 nm.[6] Although the electronic conductivity of CMK-3 is higher by about a factor of two (0.21 S cm^{-1} compared to 0.1 S cm^{-1} for the S-BMC), we observed comparable performance: slightly lower capacities (ca. 1000 mA h g^{-1}) and similarly stable cycling over the first 20 cycles. However, we have achieved this same capacity at a 5- to 10-fold higher rate with the S-BMC carbon, highlighting the importance of both the bimodal pore distribution and nano-carbon dimensions in improving electrolyte accessibility.

In summary, we have demonstrated the synthesis of spherical OMC nanoparticles of 300 nm in diameter with a 2D-hexagonal mesostructure. The material shows the highest inner pore volumes for mesoporous carbon nanoparticles of 2.32 cm^3 g^{-1} and also one of the highest surface areas of 2445 m^2 g^{-1} with a bimodal pore size distribution of large and small mesopores of 6 nm and 3.1 nm. The C/S spherical electrodes showed a high reversible charge capacity of up to 1200 mA h g^{-1} and good cycling stability. The performance of the cells could be further improved by either removing the external sulfur on the surface or by adding a thin coating of SiO_x. A comparison between nanosize and bulk carbon reveals that the excellent electrochemical properties of the cells can be largely attributed to the nanoscale morphology of the mesoporous carbon, which facilitates the preparation of homogeneous C/S composites and aids in charge transfer. This strategy is generally applicable to other C/S composites. For example, it also applies to other nanoscale carbon morphologies such as fibers, as long as they have comparable particle size, pore volume and surface area, as we shall show in subsequent work.

Experimental Section

The S-BMC nanoparticles were obtained in a two-step casting process[12a,28] as described in the text, and the C/S composites were prepared following a melt-diffusion strategy. The electrochemical performance of the Li–S cathodes was evaluated in 2325 coin cells cycled galvanostatically at room temperature against lithium metal foil, using an electrolyte comprised of a 1:1 mixture of of 1,2-dimethoxyethane (DME) and 1,3-dioxolane (DOL). This electrolyte was chosen to optimize the high rate behavior.[29] A current density of 1675 mA h g^{-1} (or 1.3 mA cm^{-2}) equivalent to full discharge or charge in 1 h was applied in both current sweep directions. For experimental details, please refer to the Supporting Information.

Received: November 7, 2011
Published online: March 1, 2012

Keywords: cathode materials · lithium–sulfur battery · nanospheres · ordered mesoporous carbon

[1] X. Ji, L. F. Nazar, *J. Mater. Chem.* **2010**, *20*, 9821 – 9826.
[2] a) J. Wang, S. Y. Chew, Z. W. Zhao, S. Ashraf, D. Wexler, J. Chen, S. H. Ng, S. L. Chou, H. K. Liu, *Carbon* **2008**, *46*, 229 – 235; b) C. Liang, N. J. Dudney, J. Y. Howe, *Chem. Mater.* **2009**, *21*, 4724 – 4730.
[3] J. Shim, K. A. Striebel, E. J. Cairns, *J. Electrochem. Soc.* **2002**, *149*, A1321 – A1325.
[4] J. Wang, L. Liu, Z. Ling, J. Yang, C. Wan, C. Jiang, *Electrochim. Acta* **2003**, *48*, 1861 – 1867.
[5] a) S.-C. Han, M.-S. Song, H. Lee, H.-S. Kim, H.-J. Ahn, J.-Y. Lee, *J. Electrochem. Soc.* **2003**, *150*, A889 – A893; b) W. Zheng, Y. W. Liu, X. G. Hu, C. F. Zhang, *Electrochim. Acta* **2006**, *51*, 1330 – 1335.
[6] X. Ji, K. T. Lee, L. F. Nazar, *Nat. Mater.* **2009**, *8*, 500 – 506.
[7] a) G. He, X. Ji, L. Nazar, *Energy Environ. Sci.* **2011**, *4*, 2878 – 2883; b) S.-R. Chen, Y.-P. Zhai, G.-L. Xu, Y.-X. Jiang, D.-Y. Zhao, J.-T. Li, L. Huang, S.-G. Sun, *Electrochim. Acta* **2011**, *56*, 9549 – 9555.
[8] B. Zhang, X. Qin, G. R. Li, X. P. Gao, *Energy Environ. Sci.* **2010**, *3*, 1531 – 1537.
[9] N. Jayaprakash, J. Shen, S. S. Moganty, A. Corona, L. A. Archer, *Angew. Chem.* **2011**, *123*, 6026 – 6030; *Angew. Chem. Int. Ed.* **2011**, *50*, 5904 – 5908.
[10] a) C. Liang, Z. Li, S. Dai, *Angew. Chem.* **2008**, *120*, 3754 – 3776; *Angew. Chem. Int. Ed.* **2008**, *47*, 3696 – 3717; b) Y. Wan, Y. Shi,

D. Zhao, *Chem. Mater.* **2008**, *20*, 932 – 945; c) H. Chang, S. H. Joo, C. Pak, *J. Mater. Chem.* **2007**, *17*, 3078 – 3088.

[11] a) C.-G. Wu, T. Bein, *Science* **1994**, *266*, 1013 – 1015; b) R. Ryoo, S. H. Joo, S. Jun, *J. Phys. Chem. B* **1999**, *103*, 7743 – 7746; c) J. Lee, S. Yoon, T. Hyeon, S. M. Oh, K. B. Kim, *Chem. Commun.* **1999**, 2177 – 2178; d) S. Jun, S. H. Joo, R. Ryoo, M. Kruk, M. Jaroniec, Z. Liu, T. Ohsuna, O. Terasaki, *J. Am. Chem. Soc.* **2000**, *122*, 10712 – 10713; e) M. Kruk, M. Jaroniec, T.-W. Kim, R. Ryoo, *Chem. Mater.* **2003**, *15*, 2815 – 2823.

[12] a) R. Liu, Y. Shi, Y. Wan, Y. Meng, F. Zhang, D. Gu, Z. Chen, B. Tu, D. Zhao, *J. Am. Chem. Soc.* **2006**, *128*, 11652 – 11662; b) Y. Meng, D. Gu, F. Zhang, Y. Shi, L. Cheng, D. Feng, Z. Wu, Z. Chen, Y. Wan, A. Stein, D. Zhao, *Chem. Mater.* **2006**, *18*, 4447 – 4464; c) X. Wang, C. Liang, S. Dai, *Langmuir* **2008**, *24*, 7500 – 7505; d) A.-H. Lu, B. Spliethoff, F. Schueth, *Chem. Mater.* **2008**, *20*, 5314 – 5319.

[13] a) C. Liang, K. Hong, G. A. Guiochon, J. W. Mays, S. Dai, *Angew. Chem.* **2004**, *116*, 5909 – 5913; *Angew. Chem. Int. Ed.* **2004**, *43*, 5785 – 5789; b) S. Tanaka, Y. Katayama, M. P. Tate, H. W. Hillhouse, Y. Miyake, *J. Mater. Chem.* **2007**, *17*, 3639 – 3645; c) J. Schuster, R. Koehn, A. Keilbach, M. Doeblinger, H. Amenitsch, T. Bein, *Chem. Mater.* **2009**, *21*, 5754 – 5762; d) L. Song, D. Feng, C. G. Campbell, D. Gu, A. M. Forster, K. G. Yager, N. Fredin, H.-J. Lee, R. L. Jones, D. Zhao, B. D. Vogt, *J. Mater. Chem.* **2010**, *20*, 1691 – 1701.

[14] a) M. Zheng, J. Cao, X. Ke, G. Ji, Y. Chen, K. Shen, J. Tao, *Carbon* **2007**, *45*, 1111 – 1113; b) M. Steinhart, C. Liang, G. W. Lynn, U. Goesele, S. Dai, *Chem. Mater.* **2007**, *19*, 2383 – 2385; c) K. Wang, W. Zhang, R. Phelan, M. A. Morris, J. D. Holmes, *J. Am. Chem. Soc.* **2007**, *129*, 13388 – 13389; d) K. Wang, P. Birjukovs, D. Erts, R. Phelan, M. A. Morris, H. Zhou, J. D. Holmes, *J. Mater. Chem.* **2009**, *19*, 1331 – 1338; e) J. Schuster, A. Keilbach, R. Köhn, M. Döblinger, T. Dörfler, T. Dennenwaldt, T. Bein, *Chem. Eur. J.* **2011**, *17*, 9463 – 9470.

[15] a) M. Zheng, G. Ji, Y. Wang, J. Cao, S. Feng, L. Liao, Q. Du, L. Zhang, Z. Ling, J. Liu, T. Yu, J. Cao, J. Tao, *Chem. Commun.* **2009**, 5033 – 5035; b) H.-J. Liu, X.-M. Wang, W.-J. Cui, Y.-Q. Dou, D.-Y. Zhao, Y.-Y. Xia, *J. Mater. Chem.* **2010**, *20*, 4223 – 4230.

[16] Z. Wang, F. Li, A. Stein, *Nano Lett.* **2007**, *7*, 3223 – 3226.

[17] Y. Yan, F. Zhang, Y. Meng, B. Tu, D. Zhao, *Chem. Commun.* **2007**, 2867 – 2869.

[18] T.-W. Kim, P.-W. Chung, I. I. Slowing, M. Tsunoda, E. S. Yeung, V. S. Y. Lin, *Nano Lett.* **2008**, *8*, 3724 – 3727.

[19] N. Tonanon, W. Intarapanya, W. Tanthapanichakoon, H. Nishihara, S. Mukai, H. Tamon, *J. Porous Mater.* **2008**, *15*, 265 – 270.

[20] Y. Fang, D. Gu, Y. Zou, Z. Wu, F. Li, R. Che, Y. Deng, B. Tu, D. Zhao, *Angew. Chem.* **2010**, *122*, 8159 – 8163; *Angew. Chem. Int. Ed.* **2010**, *49*, 7987 – 7991.

[21] H.-J. Liu, W.-J. Cui, L.-H. Jin, C.-X. Wang, Y.-Y. Xia, *J. Mater. Chem.* **2009**, *19*, 3661 – 3667.

[22] Z. Lei, N. Christov, L. L. Zhang, X. S. Zhao, *J. Mater. Chem.* **2011**, *21*, 2274 – 2281.

[23] X. Li, Y. Cao, W. Qi, L. Saraf, J. Xiao, Z. Nie, J. Mietek, J.-G. Zhang, B. Schwenzer, J. Liu, *J. Mater. Chem.* **2011**, *21*, 16603 – 16610.

[24] a) X. Ji, S. Evers, K. T. Lee, L. F. Nazar, *Chem. Commun.* **2010**, *46*, 1658 – 1660; b) C. Lai, X. P. Gao, B. Zhang, T. Y. Yan, Z. Zhou, *J. Phys. Chem. C* **2009**, *113*, 4712 – 4716; c) W. Liu, R. D. Vidić, T. D. Brown, *Environ. Sci. Technol.* **1998**, *32*, 531 – 538; d) Y. Yang, M. T. McDowell, A. Jackson, J. J. Cha, S. S. Hong, Y. Cui, *Nano Lett.* **2010**, *10*, 1486 – 1491.

[25] a) M.-S. Song, S.-C. Han, H.-S. Kim, J.-H. Kim, K.-T. Kim, Y.-M. Kang, H.-J. Ahn, S. X. Dou, J.-Y. Lee, *J. Electrochem. Soc.* **2004**, *151*, A791 – A795; b) Y. J. Choi, D. J. L. B. S. Jung, J. H. Jeong, K. W. Kim, H. J. Ahn, K. K. Cho, H. B. Gu, *Phys. Scr.* **2007**, 62; c) H. Wang, Y. Yang, Y. Liang, J. T. Robinson, Y. Li, A. Jackson, Y. Cui, H. Dai, *Nano Lett.* **2011**, *11*, 2644 – 2647; d) J. Wang, J. Yang, J. Xie, N. Xu, *Adv. Mater.* **2002**, *14*, 963 – 965; e) J. Hassoun, B. Scrosati, *Angew. Chem.* **2010**, *122*, 2421 – 2424; *Angew. Chem. Int. Ed.* **2010**, *49*, 2371 – 2374; f) J. Hassoun, B. Scrosati, *Adv. Mater.* **2010**, *22*, 5198 – 5201.

[26] X. Ji, S. Evers, R. Black, L. F. Nazar, *Nat. Commun.* **2011**, *2*, 325.

[27] K. T. Lee, X. Ji, T. Yim, L. F. Nazar, unpublished results.

[28] B. T. Holland, C. F. Blanford, A. Stein, *Science* **1998**, *281*, 538 – 540.

[29] a) E. Peled, Y. Sternberg, A. Gorenshtein, Y. Lavi, *J. Electrochem. Soc.* **1989**, *136*, 1621 – 1625; b) Y. V. Mikhaylik, I. Kovalev, R. Schock, K. Kumaresan, J. Xu, J. Affinito, *ECS Trans.* **2010**, *25*, 23 – 34.

